NJC

ROYAL SOCIETY OF CHEMISTRY

PAPER

View Article Online
View Journal

Cite this: DOI: 10.1039/d1nj04103g

Effects of external parameters and mass-transfer on the glucose oxidation process catalyzed by Pd–Bi/Al_2O_3†

Mariya P. Sandu, [ab] Mikhail A. Kovtunov, [a] Nikolay V. Gromov [c] and Irina A. Kurzina *[a]

Received 26th August 2021,
Accepted 27th October 2021

DOI: 10.1039/d1nj04103g

rsc.li/njc

The catalytic properties of a bimetallic 3.5% Pd–2.4% Bi catalyst supported on Al_2O_3 were studied in a glucose oxidation reaction in sodium gluconate at various pHs, temperatures and [Glu] : [Pd] ratios. It was found that pH 9 and temperature 60 °C are the best conditions for the Pd_3Bi/Al_2O_3 catalytic system. These reaction parameters contribute to obtaining sodium gluconate with 56.6% yield while maintaining a selectivity of 99.9%. The calculated activation energy was 67.7 kJ mol^{-1}. The oxygen transfer rate investigation allowed us to conclude that the reaction proceeds in a kinetic mode. The catalyst showed activity and stability in three catalytic cycles (X_{Glu} = 56.6–62.8, S_{SGlu} > 99.9%). The decrease in catalytic activity in the fourth and fifth catalytic cycles is associated with a change in the valence-phase state of the catalyst surface established using XPS.

Introduction

The global reserves of fossil raw materials are gradually depleting, and the use of natural resources becomes more relevant. Renewable raw materials present the major source of valuable organic compounds used for the chemical industry.[1,2] Carbohydrates obtained from plant biomass constitute a solid foundation for the synthesis of many useful chemicals.[3] One of these components is gluconic acid, the industrial production of which is approximately 100 000 tons per year.[4] Gluconic acid is non-toxic, biodegradable and capable of forming chelate complexes with cations of various metals. These properties have enabled gluconic acid to be implemented in the food industry as a disintegrant, preservative, and an agent that prevents the precipitation of calcium and iron salts in the production of fruit juices.

Gluconate ions easily bind di- and trivalent metal cations thus serving as a detergent in metallurgy and household cleaning.[5,6] Also, calcium, iron, zinc, and magnesium gluconates are used in medical therapy for the treatment of diseases caused by the lack of these microelements in the body.[6–8] Gluconic acid and its salts are also implemented in the construction, printing, leather, textile, and paper industries.[9,10]

The main industrial method for the production of gluconic acid is the fermentation of glucose by various bacterial genus, such as *Aspergillus*,[11,12] *Penicillum*,[13,14] *Gluconobacter*, *Pseudomonas*, *Acetobacter*, *Aureobasidium*, *Zymomonas*, *etc.*, which can release an active enzyme.[11–24] However, the enzymatic method is complicated by several technological aspects. It is associated with strict control of the fermentation conditions and the nutrient medium composition, the impossibility of reusing microorganisms, large volumes of waste, and challenging separation of the desired product from the reaction mass.[1,25] Also, the biotechnological fermentation is characterized by a low rate, since the accumulation of gluconic acid in the reaction medium suppresses the vital activities of microorganisms.[26,27]

In order to overcome the disadvantages of traditional synthesis, other methods are being devised. The oxidation of glucose with molecular oxygen in the presence of heterogeneous catalysts seems promising.[28] The supported platinum group metals (*e.g.* Pt and Pd) that demonstrate stability in an aqueous medium have proven to be effective in this reaction.

However, monometallic systems tend to deactivate and show lower efficiency than bimetallic catalysts based on palladium or platinum promoted with various additives, such as, Bi, Tl, Co, Sn, and Te.[29–36] Evidently, the addition of the second metal prevents the oxidation of the catalyst's surface thus protecting the active sites.[33] However, an important requirement for achieving high yield and selectivity is the selection of optimal production parameters – temperature and pH. Abbadi and van Bekkum studied the effects of pH and temperature on glucose oxidation using a 5% Pt/C catalyst.[37] In this case, without pH

[a] National Research Tomsk State University, 36 Prospekt Lenina, 634050, Tomsk, Russia. E-mail: kurzina99@mail.ru
[b] Siberian State Medical University, 2 Moskovsky Trakt, 634050, Tomsk, Russia
[c] Boreskov Institute of Catalysis SB RAS, 5 Prospekt Lavrentieva, 630090, Novosibirsk, Russia

† Electronic supplementary information (ESI) available. See DOI: 10.1039/d1nj04103g

control and at pH ~ 5, catalyst poisoning by gluconic acid was observed, and inhibition of the oxidation process occurred. At pH 7, the initial reaction rate decreased twice as fast compared to pH 9. Investigation shows that a temperature increase from 50 °C to 65 °C does not greatly affect the initial reaction rate or selectivity. However, due to the weak adsorption of poisoning substances at 65 °C, the reaction proceeded to a greater extent. Önal *et al.* achieved an increase of the initial reaction rate by a factor of 3.2 with a pH increase from 7 to 9.5 on the Au/C catalyst.[32] The unsupported suspended gold particles, which were studied by Yin *et al.*,[38] allowed the authors to achieve 99% selectivity towards gluconic acid. In this case, the glucose conversion was 33% at pH 7 and 78% at pH 9. A temperature increase from 283 K to 323 K led to a fourfold increase in the reaction rate without the formation of any by-products.

Thus, the external parameters of the reaction, namely, pH and temperature, can significantly affect the rate of reaction, its completeness, and selectivity towards the target product in the presence of catalysts of various compositions. The purpose of this work was to study the effects of the pH level, temperature, and loading of the catalyst on the glucose oxidation into gluconic acid on the Pd–Bi/Al_2O_3 catalyst with a Pd : Bi atomic ratio of 3 : 1.

Materials and methods

Catalyst preparation

Microspherical γ-Al_2O_3 ("SKTB Katalizator", Russia) with a surface area of 174 m^2 g^{-1} and a total pore volume of 0.35 cm^3 g^{-1} was used as a support. The alumina powder was sifted to obtain a particle fraction of 125–250 μm.

Pd/Al_2O_3, Bi/Al_2O_3, and Pd3 : Bi1/Al_2O_3 (where 3 : 1 is the Pd : Bi atomic ratio) samples were prepared according to a technique described earlier.[39] The 3 : 1 ratio was chosen based on the results obtained in a previous study.[40] To synthesize the Pd3 : Bi1/Al_2O_3 sample, the Al_2O_3 support underwent co-impregnation using $Pd(acac)_2$ and $Bi(ac)_3$ dissolved in acetic acid. After impregnation, excess solvent was removed using a rotary evaporator. Thereafter the catalyst powder was dried in a vacuum cabinet and a three-stage temperature treatment was carried out in flows of argon (500 °C), oxygen (350 °C), and hydrogen (500 °C). The monometallic Pd/Al_2O_3 and Bi/Al_2O_3 catalysts were prepared similarly using either $Pd(acac)_2$ or $Bi(ac)_3$ as a precursor. Then Pd3 : Bi1/Al_2O_3 was chosen for further investigation as a sample of interest. Pd/Al_2O_3 and Bi/Al_2O_3 were used as comparison samples. While referring to the catalytic samples, Pd/Al_2O_3, Bi/Al_2O_3, and Pd3 : Bi1/Al_2O_3 are further designated as Pd, Bi and Pd3 : Bi1, respectively.

Surface characterization

The surface area, average pore size and total pore volume of the obtained samples were determined using a TriStar 3020 analyser (Micromeritics, USA). Approximately 100 mg of each sample was degassed for 2 hours using VacPrep 061 (Micromeritics, USA) before the measurement. The Brunauer–Emmett–Teller method was implemented for the surface area value calculation, and the Barrett–Joyner–Halenda method was used for the pore size and pore volume determination.

X-ray fluorescence analysis (XRF)

Lab Center XRF-1800 (Shimadzu, Japan) was used for qualitative and quantitative analyses of the samples obtained. The X-ray tube with a voltage of 40 kV, an amperage of 95 mA, and an aperture of 3 mm was used for qualitative and quantitative analyses. Measurements were conducted at a scanning step of 8 degree per min. The device error is 10%.

Transmission electron microscopy and energy dispersive spectrometry (TEM–EDS)

JEOL JEM-2100F (JEOL Ltd, Akishima, Tokyo, Japan) was used to obtain TEM-images of the catalysts obtained. The microscope was equipped with an electron gun with the field emission of the cathode (FEG), a high-resolution pole tip (point resolution of 0.19 nm) and a JEOL JED-2300 Analysis Station Spectrometer (JEOL Ltd, Akishima, Tokyo, Japan). The samples were suspended in ethanol using an ultrasonic bath and afterwards deposited on the carbon coated copper TEM-grids (3.05 mm in diameter, 300 mesh).

Scanning electron microscopy and energy dispersive spectroscopy (SEM–EDS)

SEM-images were made using a Tescan MIRA 3 equipped with an energy dispersive spectrometer Oxford Instruments Ultim Max 40 at an accelerating voltage of 20 kV. The equipment was provided by the Analytical Center of Natural Systems' Geochemistry, TSU.

X-ray photoelectron spectroscopy (XPS)

XPS patterns were obtained using a PHI 5000 VersaProbe-II (ULVAC-PHI, Chigasaki, Kanagawa, Japan). The Al 2p line was taken as an internal standard at 74.5 eV during the analysis of γ-Al_2O_3. The accuracy of binding energy measurements was ± 0.1 kV. The XPS spectra were processed using standard CasaXPS software (version 2.3.22PR1.0, 2018, Casa Software Ltd, UK).

Research of catalytic properties

Liquid-phase glucose oxidation was conducted within a temperature range of 20–90 °C and a pH range of 6–12 in a static reactor (V = 25 ml, atmospheric pressure). The pH was maintained with a peristaltic pump by feeding 3 M NaOH (LenReactiv, St. Petersburg, Leningrad region, Russia, 99%); the pH control was carried out using a combined glass electrode. The initial glucose concentration was about 0.6 mol L^{-1}, and the oxidizing agent (oxygen) was supplied at a rate of 10 ml min^{-1}. The reaction was carried out for 150 min with continuous stirring (1000 rpm). During neutralization of the obtained product with alkali, a derivative of gluconic acid is formed, namely sodium gluconate (SGlu). The catalytic properties were characterized using glucose conversion (X_{Glu}), sodium gluconate yield (Y_{SGlu}), selectivity towards sodium gluconate (S_{SGlu}) and turnover frequency (TOF) and calculated according to the formulas (1–4) presented in the ESI.†

High performance liquid chromatography (HPLC)

A Zorbax NH2 250 × 4.6 mm, 5 μm (Agilent, USA) column was used for HPLC-analysis performed at 55 °C using a refractive index detector. A mixture of phosphate buffer and acetonitrile (volume ratio of 1 : 4) was used as a mobile phase. The samples were injected three times. Next, the average concentration was found and the error was calculated using Student's *t*-test with a confidence level of 0.95 for three measurements (N = 3).

Results and discussion

Metal content and texture characterization

X-ray fluorescence analysis showed that the Pd3 : Bi1 catalyst powder contains 3.5 mass% of Pd and 2.4 mass% of Bi, which grants the Pd : Bi ratio of 2.86. The specific surface area determined by the BET method is 135 $m^2\ g^{-1}$. The total pore volume is 0.263 $cm^3\ g^{-1}$.

Investigation by electron microscopy

Particle micrographs of Pd and Pd3 : Bi1 catalysts were obtained using a transmission electron microscope (Fig. 1). The images allow us to conclude that the catalyst particles of spherical shape are uniformly distributed over the support surface. According to the histogram of the particle size distribution shown in Fig. 1, the particle diameter of the monometallic and bimetallic samples varies from 1 to 9 nm. The average particle diameter of the Pd and Pd3 : Bi1 catalysts is 4.3 and 4.0 nm, respectively. Therefore, the addition of bismuth in such quantities does not cause the particle size increase.

Elemental analysis of the catalyst particles was carried out using EDS. Fig. 2 shows that palladium and bismuth atoms are uniformly distributed over the catalyst surface. This allows us to assume that palladium and bismuth form bimetallic particles. However, these data are not sufficient to conclude safely that there is an interaction between two metals, and XPS will be required to confirm this assumption.

Fig. 3 shows the SEM-image of a single support granule (Fig. 3a) and the elemental mapping performed using EDS (Fig. 3b). Palladium and bismuth particles are uniformly distributed over the entire surface of the support granule and are also deposited in the pores. Palladium forms only a few regions with relatively high concentrations. The results of local point scanning are presented in the ESI† (Fig. S1 and Table S1).

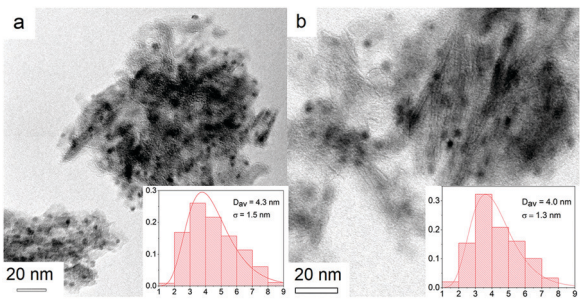

Fig. 1 TEM-images of Pd (a) and Pd3 : Bi1 (b) samples.

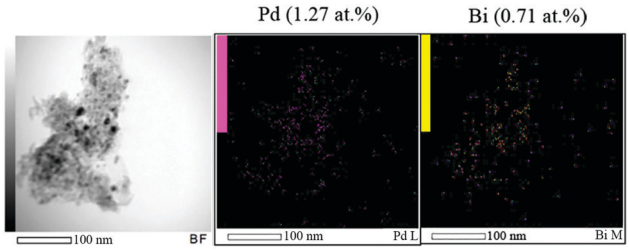

Fig. 2 Palladium and bismuth distribution over the support surface for the Pd3 : Bi1 sample.

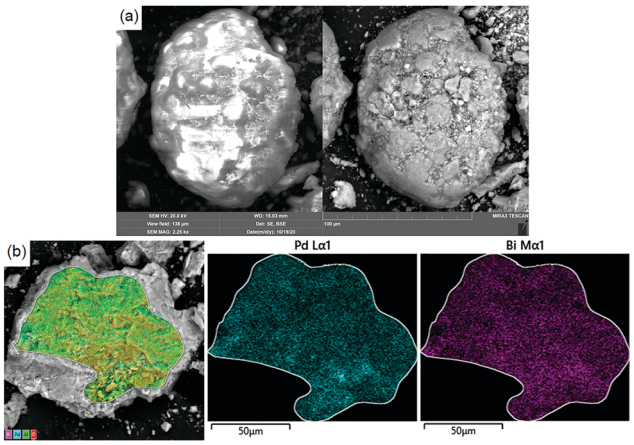

Fig. 3 SEM-images of the catalyst granule (a) and element mapping (b) for the Pd3 : Bi1 sample.

X-ray photoelectron spectroscopy (XPS)

The surface structural-phase state of mono- and bimetallic samples was investigated using XPS. To determine the state of metal particles, peak deconvolution in XPS-patterns was performed. The XPS-profile for the Pd sample (Fig. 4) is presented as two asymmetric peaks associated with the Pd $3d_{3/2}$ and Pd $3d_{5/2}$ states at 340.7 eV and 335.4 eV, respectively. The Pd $3d_{5/2}$ peak maximum is used for comparison of binding energies.[41] Pd^0 and $Pd(II)_{ads}$ phases corresponding to the binding energies of 335.2 eV and 336.4 eV, respectively, were found in the XPS-pattern of the monometallic sample for core-level Pd $3d_{5/2}$ (Table 1).[42,43] The XPS-pattern of the valent level Bi $4f_{7/2}$ for the Bi/Al_2O_3 sample peaks at 156.8 eV and 158.0 eV

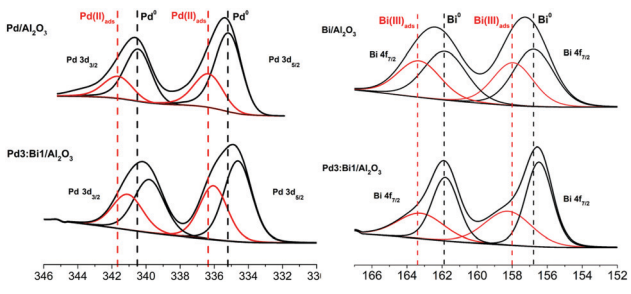

Fig. 4 XPS-patterns of Pd 3d (a) and Bi 4f (b) states for mono- and bimetallic samples.

Table 1 Binding energies for Pd $3d_{5/2}$ and Bi $4f_{7/2}$ core-levels and phase percentage for the obtained samples

Sample		Pd	Bi	Pd3 : Bi1
Pd $3d_{5/2}$, eV		Pd^0 335.2, $Pd(II)_{ads}$ 336.4	—	Pd^0 334.6, $Pd(II)_{ads}$ 336.0
Bi $4f_{7/2}$, eV		—	Bi^0 156.8, $Bi(III)_{ads}$ 158.0	Bi^0 156.5, $Bi(III)_{ads}$ 158.2
Phase content, at%	Pd^0	68.8	—	60.0
	$Pd(II)_{ads}$	31.2	—	40.0
	Bi^0	—	57.1	58.8
	$Bi(III)_{ads}$	—	42.9	41.2

correspond to the Bi^0 and $Bi(III)_{ads}$ phases, respectively.[44,45] Oxidized state formation is caused by specific interaction between organometallic precursors and the alumina surface during the catalyst preparation stage. It can also occur due to palladium particle oxidation by atmospheric oxygen, which leads to oxide film formation and blockage of the active sites.[46,47] It is worth noting that the actual Pd : Bi atomic ratio is lower than the ratio determined *via* XRF (2.86) and is equal to 2.1. This difference is caused by the fact that bismuth covers some of the palladium surface atoms thus preventing their detection by XPS.[48] Earlier, using USPEX Evolution-Code, we modelled palladium–bismuth nanoclusters and found that bismuth is deposited on the surface of the palladium core, forming an inverted 'crown-jewel' morphology with an amount of bismuth introduced up to 40 at% in relation to palladium. A further increase in the introduced bismuth content contributes to the formation of a 'core–shell' structure. Thus, we suppose that the inverted 'crown-jewel' structure is the characteristic of the particles that constitute the Pd3 : Bi1/Al_2O_3 catalyst.[40]

For the Pd3 : Bi1 sample, the XPS-profile shows a peak shift for Pd^0 and Bi^0 to lower values compared to the monometallic samples. This negative binding energy shift is probably associated with the interaction between palladium and bismuth that takes place during the high temperature heat treatment stage of the catalyst and leads to the redistribution of the electron density between metal atoms.[49–51] A positive shift for $Bi(III)_{ads}$ and negative shift for $Pd(II)_{ads}$ are likely due to the electron transfer from the $Bi(III)_{ads}$ to $Pd(II)_{ads}$ phase.[52] The excess of the electron density on Pd atoms, apparently, should facilitate the adsorption of glucose since the hydrogen atom involved in glucose binding is characterized by a partial positive charge created by oxygen in glucose molecules.

Research of catalytic properties

Influence of pH. The Pd3 : Bi1 catalyst was tested in the glucose oxidation reaction for 150 min at a pH varied from 6 to 12 and at a temperature of 60 °C. The reaction was also conducted without pH control. During an uncontrolled pH-process, the reaction proceeded for a short time until pH 3.4 was reached and practically stopped after that. The gluconic acid yield was less than 1%. At a pH level of 6–7, the conversion of glucose slightly increased and reached 3.6% and 17.1%, respectively (Table 2). The kinetic dependence of glucose conversion on time at different pH values is shown in Fig. 5.

It is assumed that in acidic and neutral media, the low activity of the catalyst is associated with surface poisoning by oxygen, which leads to the formation of the inactive layer of palladium oxide, and/or by the obtained gluconic acid. This poisoning of the catalyst's surface by gluconic acid was described by Abbadi *et al.* during the study of Pt/C catalysts for glucose oxidation at pH $\leq$ 7.[37] We will discuss the decrease in activity at low pH in more detail in the section 'Post-catalytic investigation'. A pH increase to 8–9 caused a significant conversion increase to 51.0% and 56.6%, respectively. In the weakly alkaline medium, the active surface of the catalyst is regenerated due to the dissociation of gluconic acid complexes with the gluconate ion formation.[53] With a pH increase to 10–11, the conversion of glucose continued to increase, however, in addition to sodium gluconate, fructose was found as a by-product associated with glucose isomerization in alkaline media.[54] At pH 11, the selectivity towards gluconate ion decreased to 80.8%. In a

Table 2 The influence of pH on glucose conversion, sodium gluconate yield, and reaction selectivity

pH level	X_{Glu}, %	Y_{SGlu}, %	S_{SGlu}, %	S_{Fru}, %	S_{other}, %	TOF, s^{-1}
6	3.6	3.6	>99.9	<0.1	—	0.0163
7	17.1	17.1	>99.9	<0.1	—	0.0774
8	51.0	51.0	>99.9	<0.1	—	0.2307
9	56.6	56.6	>99.9	<0.1	—	0.2561
10	72.9	68.7	94.3	6.7	—	0.3298
11	78.3	63.3	80.8	19.2	—	—[a]
12	88.1	38.1	43.2	12.9	43.9	—[a]

[a] Difficult to assess since the degradation of glucose in a highly alkaline medium is not a catalytic process. Reaction conditions: T = 60 °C, stirring speed = 1000 rpm, C (glucose) = 0.017 mol, m (catalyst) = 0.0108 g, oxygen supply rate = 10 ml min^{-1}.

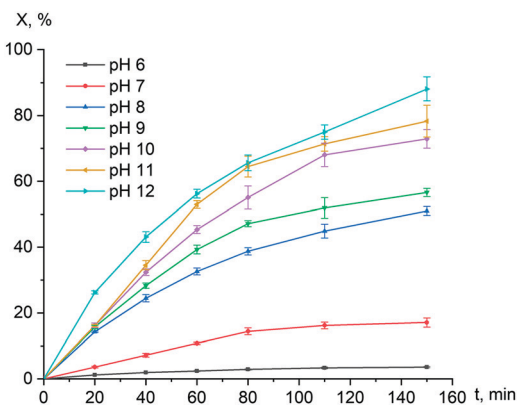

Fig. 5 Glucose conversion *versus* time at different pH levels. Reaction conditions: T = 60 °C, stirring speed = 1000 rpm, C (glucose) = 0.017 mol, m (catalyst) = 0.0108 g, oxygen supply rate = 10 ml min^{-1}.

strongly alkaline medium (pH 12), both glucose and reaction products were destroyed, and the selectivity towards sodium gluconate was 43.2%. The by-product formation was intensive at this point and was presented by formic, oxalic, and glyoxalic acids, as well as by ethyleneglycol. Thus, the optimum pH value for the formation of gluconate ion is 9, since it provides a high yield of sodium gluconate without the formation of any by-products. The decrease of selectivity caused by isomerization and by-product formation was described by Önal *et al.* for a Au/C catalyst at high pH.[32] The highest activity was achieved by the authors at pH 9–10 and was equal to 0.7 s^{-1}.

Influence of temperature

Catalytic tests of the Pd3 : Bi1 sample were conducted in the temperature range from 20 to 60 °C, at a pH level of 9 and a [Glu] : [Pd] ratio of 5000 : 1. At a temperature of 20 °C (room temperature), the reaction barely proceeded, and by the end point of time the conversion of glucose reached 1.7% (Table 3).

A temperature increase to 30 °C led to an increase of the reaction rate by a factor of 4 compared to the reaction conducted at room temperature. In this case, the conversion reached to 6.9%. At 40 °C, the reaction rate increased another 2.5 times. A temperature increase to 60 °C led to a glucose conversion value of 56.6%. Within the temperature range of 20–60 °C, the reaction proceeded selectively without any by-product formation or at concentrations that were below the detection limit. For 70 °C and 80 °C, formation of fructose as a by-product was observed. At 90 °C the by-product formation became significant and included formic, oxalic, and glyoxalic acids, as well as ethylene glycol. The apparent activation energy was calculated by a graphical method using the Arrhenius equation, which was 67.7 kJ mol^{-1}. This value was calculated within the temperature range of 20–60 °C since there were no by-products detected. The activation energy for the Pd–Bi/C system was previously determined by Fan *et al.* in the case of oxidation of ribose to ribonate: the value calculated by the authors was 71.3 kJ mol^{-1}, which is comparable to the numbers obtained in this work.[55] A glucose to gluconic acid reaction at a high oxygen pressure catalyzed by alumina-supported gold was studied by Prüße *et al.* and was characterized by an energy barrier of 54 kJ mol^{-1}.[56]

Table 3 The temperature influence on glucose conversion, sodium gluconate yield, and reaction selectivity

T, °C	X_{Glu}, %	Y_{SGlu}, %	S_{SGlu}, %	S_{Fru}, %	S_{other}, %	TOF, s^{-1}
20	1.7	1.7	>99.9	<0.1	—	0.0077
30	6.9	6.9	>99.9	<0.1	—	0.0312
40	17.6	17.6	>99.9	<0.1	—	0.0796
50	25.0	25.0	>99.9	<0.1	—	0.1131
60	56.6	56.6	>99.9	<0.1	—	0.2561
70	47.4	36.9	78.0	22.0	—	—
80	55.2	33.2	59.9	40.1	—	—
90	65.2	16.5	25.3	33.9	40.8	—

Reaction conditions: pH = 9, stirring speed = 1000 rpm, C (glucose) = 0.017 mol, m (catalyst) = 0.0108 g, oxygen supply rate = 10 ml min^{-1}.

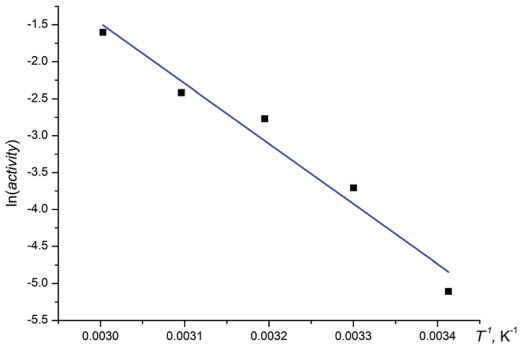

Fig. 6 Arrhenius plot for the determination of the apparent activation energy. Reaction conditions: pH = 9, stirring speed = 1000 rpm, C (glucose) = 0.017 mol, m (catalyst) = 0.0108 g, oxygen supply rate = 10 ml min^{-1}.

A decrease in glucose conversion at 70 °C is associated with inhibition of the gluconate ion formation process and activation of side pathways, which are accompanied by the formation of by-products in the oxidation process. However, at 80 °C and 90 °C, an increase in glucose conversion occurs, since an increase in temperature promotes higher yields for by-products. A similar decrease in glucose conversion at 70 °C was observed by Önal and his colleagues when studying catalysts with Au/C composition in the oxidative reaction of glucose.[32] However, carbon-supported gold catalysts lead to the formation of other by-products when the temperature increases above 60 °C, such as mannose, glycolaldehyde, sorbitol and maltose. For activation energy calculation, a temperature range of 20–60 °C was used since higher temperatures favour intense by-product formation. The Arrhenius plot for activation energy is shown in Fig. 6.

Besson and his colleagues proposed a scheme of oxidative glucose dehydrogenation.[33] According to this scheme, two hydrogen atoms at the anomeric carbon atom and at the hemiacetal hydroxyl group are chemisorbed by the active sites of palladium, which results in lactone formation (Fig. 7). The hydroxogroups present in the alkaline medium allow the lactone decyclization with gluconate ion formation. At the same time, bismuth chemisorbs the oxygen, thus protecting palladium from oxidation. Chemisorbed hydrogen and oxygen atoms then

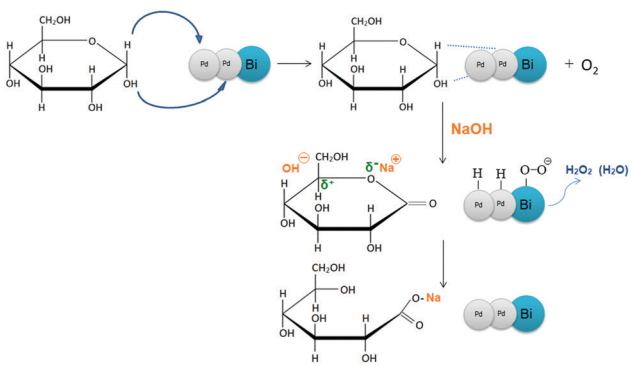

Fig. 7 Oxidative dehydration scheme proposed by Besson *et al.*

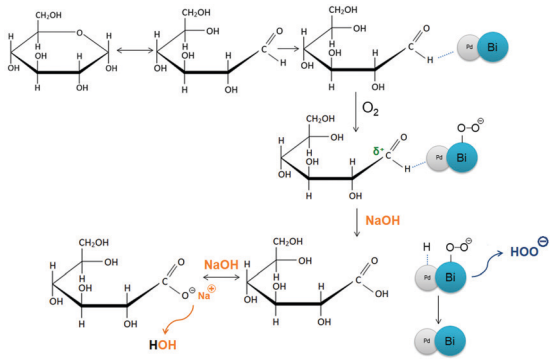

Fig. 8 A proposed glucose oxidation mechanism for the Pd–Bi catalytic system.

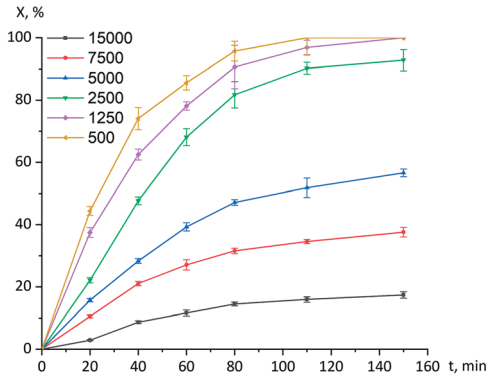

Fig. 9 Glucose conversion *versus* time at different glucose:palladium molar ratios. Reaction conditions: T = 60 °C, pH = 9, stirring speed = 1000 rpm, C (glucose) = 0.017 mol, oxygen supply rate = 10 ml min^{-1}.

form water (or hydrogen peroxide) and leave the catalyst surface, which returns the active sites to an unoccupied state.

Given that the reaction does not proceed at low pH, we suggest a slightly different path for this process. During the reaction, especially at higher temperatures, the glucose cycle might open. The glucose molecule is then adsorbed on the palladium active sites *via* aldehyde group hydrogen (Fig. 8). Hydroxogroups present in the medium bind with the carbon atom of the aldehyde group, which leads to gluconate ion desorption. Chemisorbed hydrogen and oxygen then form water or hydrogen peroxide molecules and leave the catalyst surface as described above.

Oxygen transfer study

To evaluate the impact of the mass transfer processes on the glucose oxidation kinetics in the presence of the Pd3 : Bi1 catalyst, it is necessary to estimate the rates of interfacial gas–liquid and liquid–solid oxygen transfer under the reaction conditions and to compare these data with the reaction rates evaluated from the experimental parameters. It should be noted, however, that since the numerical calculation of interfacial mass transfer parameters for polydispersed systems is quite challenging, the aim of our work is to evaluate at least the order of their magnitude. The estimated data on reaction rates and oxygen transfer can be found in Table 4. The parameters presented were calculated according to the formulas presented in the ESI.†[57,58]

The results obtained let us conclude that the rates of oxygen diffusion from liquid to solid are higher compared to the reaction rates by one or two orders of magnitude and do not influence the reaction kinetics. The rates of reaction and oxygen dissolution are comparable in the order of magnitude, but in several cases the reaction rate is 2–4 times greater. This phenomenon might be explained by the fact that the oxygen is supplied not only from the solution, but also in its undissolved molecular form, which is possibly caused by the high stirring speed (Fig. 9).

At ratios of 2500, 5000, and 7500, a complete conversion of glucose was not achieved; however, no by-product formation was observed (Table 5). At a 15 000 molar ratio, the formation of fructose occurs, which is due to the glucose isomerization. The highest activity of ~0.45 s^{-1} was achieved at a [Glu] : [Pd] molar ratio of 1250–500. To compare the catalytic activity with the data presented in other studies, the average reaction rates were calculated. Wenkin *et al.* tested a Pd3 : Bi1/C catalyst at a 16 000 [Glu] : [Pd] molar ratio and achieved an average reaction rate of 0.062 mol of gluconic acid (g Pd)$^{-1}$ min^{-1} with a gluconic acid yield of 10% after 4 h of the experiment.[59] In this work, the average reaction rate at a 15 000 [Glu] : [Pd] molar ratio was 2.3 times higher and was equal to 0.146 mol of sodium gluconate (g Pd)$^{-1}$ min^{-1}. The highest reaction rates, however, were achieved at a 2500–5000 [Glu] : [Pd] molar ratio

Table 4 Initial reaction rates (R) revealed in the presence of the Pd3 : Bi1 sample, the calculated rates of oxygen dissolution (I) and external diffusion (J)

Glu : Pd molar ratio	$R \times 10^6$, mol l^{-1} s^{-1}	$(R{\cdot}V) \times 10^6$, mol s^{-1}	$I \times 10^6$, mol s^{-1}	$J \times 10^6$, mol s^{-1}
15 000	14.3	0.4	1.2	10.8
7500	35.1	1.0		21.6
5000	72.1	2.0		32.4
2500	97.4	2.7		64.8
1250	146.9	4.1		129.5
500	163.3	4.5		323.8

Reaction conditions: T = 60 °C, pH = 9, stirring speed = 1000 rpm, C (glucose) = 0.017 mol, oxygen supply rate = 10 ml min^{-1}.

Table 5 Quantitative characteristics of the glucose oxidation reaction at various glucose : palladium molar ratios

Glu : Pd molar ratio	X_{Glu}, %	Y_{SGlu}, %	S_{SGlu}, %	TOF, s^{-1}	Average rate (mol(SGlu)/(g Pd) min), after 150 min
15 000	17.4	16.0	92.0	0.0787	0.146
7500	37.6	37.6	>99.9	0.1701	0.171
5000	56.6	56.6	>99.9	0.2561	0.172
2500	92.8	92.8	>99.9	0.4198	0.141
1250	100.0	95.5	95.5	0.4519	0.072
500	100.0	86.2	86.2	0.4519	0.026

Reaction conditions: T = 60 °C, pH = 9, stirring speed = 1000 rpm, C (glucose) = 0.017 mol, oxygen supply rate = 10 ml min^{-1}.

Table 6 Quantitative characteristics of the glucose oxidation reaction in the presence of a Pd3 : Bi1 catalyst over five catalytic cycles

Number of cycle	X_{Glu}, %	Y_{SGlu}, %	S_{SGlu}, %	TOF, s^{-1}
1	56.6	56.6	>99.9	0.2561
2	62.8	62.8	>99.9	0.2841
3	57.3	57.3	>99.9	0.2592
4	47.3	45.9	97.0	0.2140
5	43.7	41.2	94.3	0.1977

Reaction conditions: T = 60 °C, pH = 9, stirring speed = 1000 rpm, C (glucose) = 0.017 mol, m (catalyst) = 0.0108 g, oxygen supply rate = 10 ml min^{-1}.

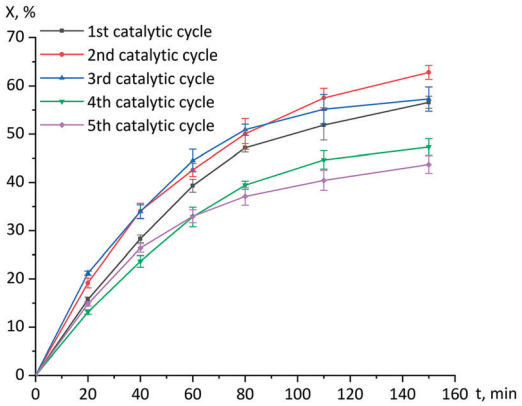

Fig. 10 Time dependence of glucose conversion in five catalytic cycles in the presence of a Pd3 : Bi1 catalyst. Reaction conditions: T = 60 °C, pH = 9, stirring speed = 1000 rpm, C (glucose) = 0.017 mol, m (catalyst) = 0.0108 g, oxygen supply rate = 10 ml min^{-1}.

and equal to approximately 0.170 mol of sodium gluconate (g Pd)$^{-1}$ min^{-1}.

Evaluation of the stability in five catalytic cycles for Pd3 : Bi1 was performed at the [Glu] : [Pd] molar ratio 5000 : 1 (Table 6 and Fig. 10). The catalytic activity changed insignificantly during the first three catalytic cycles.

Interestingly, the values reached during the second and the third cycles exceed those for the first reaction cycle. In this case, the conversion of glucose reached 56–63% without any by-product formation (see the "Post-catalytic investigation of the Pd3 : Bi1 sample" section for details). In the fourth and fifth cycles, glucose conversions decreased to 47% and 44%, respectively. Selectivity for sodium gluconate decreased only slightly. The only by-product found after the last two oxidation cycles is glucose's structural isomer – fructose.

Post-catalytic investigation of the Pd3 : Bi1 sample

The catalyst was extracted from the reaction medium at pH 3.4, when no alkali was added, rinsed with distilled water, and dried at room conditions. Then the catalyst surface was investigated by XPS for the Pd 3d core level (as a component on the surface of which the substrate was adsorbed). The predominance of the oxidized state of Pd(II)$_{ads}$ (336.7 eV) and the PdC intermediate carbide phase (335.5 eV) were observed in the XPS pattern as shown in Fig. 11.[42,43,60]

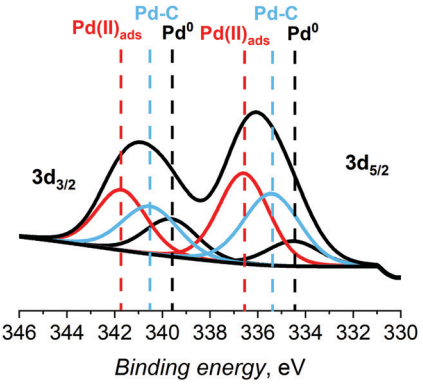

Fig. 11 XPS profile for the Pd3 : Bi1 catalyst after the experiment at pH 3.4.

Table 7 Results of the XPS analysis after experiment at pH 34

Phase	Binding energy, eV	Phase content, at%
Pd^0	334.6	18.8
PdC	335.5	38.3
Pd(II)$_{ads}$	336.6	42.9

Palladium in the zero valence-state was found in an insignificant amount (18.8 at%). In this case, the number of active centers was insufficient for substrate adsorption and reaction product desorption. Thus, we confirm the assumption that in the catalytic process at pH < 7, the active surface of palladium is poisoned by adsorption of the intermediate product and oxidative deactivation. The peaks positions and phase contents are given in Table 7.

Similarly, the catalyst surface was examined by the XPS method after first, second, and fourth catalytic tests at pH 9. The residual amount of metal on the catalyst surface was studied by XRF. The palladium and bismuth contents were 3.4 mass% and 2.3 mass%, respectively. An insignificant decrease in the proportion of metals in the catalyst powder may be associated with an error in measuring the device or leaching of palladium and bismuth into the reaction mixture.

XPS was used to investigate the structural-phase properties of the sample after the first catalytic cycle (Table 8). Fig. 12 shows the XPS patterns for Pd 3d and Bi 4f bond energies. It was found that palladium(II) oxide may undergo oxidation forming palladium(IV) oxide, which is represented by a small peak at 337.8 eV. It occurs in accordance with the following equation:[61–63]

$$PdO + H_2O \leftrightarrows PdO_2 + 2H^+ + 2e^-$$

Bi^{3+} ions undergo hydrolysis in aqueous solutions, which is followed by the formation of hydroxocomplexes and their polymerization. These processes depend on the pH level of the solution. Bismuth hydrolysis can also be described in terms of BiO^+ ion formation. For instance, $Bi(OH)_3$ formed during hydrolysis can lose one H_2O molecule:

$$Bi(OH)_3 \rightarrow BiOOH + H_2O$$

Table 8 Pd $3d_{5/2}$ and Bi $4f_{7/2}$ binding energies and element atomic percentage of the Pd3 : Bi1 sample before and after the catalytic test

Sample		Before catalysis	After 1st catalysis	After 4th catalysis
Pd $3d_{5/2}$, eV		Pd^0 334.6, $Pd(II)_{ads}$ 336.0	Pd^0 334.6, $Pd(II)_{ads}$ 336.0, Pd^{2+} 337.8	Pd^0 334.5, $Pd(II)_{ads}$ 336.0, Pd^{2+} 337.9
Bi, $4f_{7/2}$, eV		Bi^0 156.5, $Bi(III)_{ads}$ 158.2	Bi^0 156.8, $Bi(III)_{ads}$ 158.0, BiO^+ 158.6	$Bi(III)_{ads}$ 158.0, BiO^+ 158.8, Bi^{3+} 159.8, Bi^{5+} 160.7
Element content, at%	Pd	1.23	0.46	0.31
	Bi	0.58	0.15	0.04

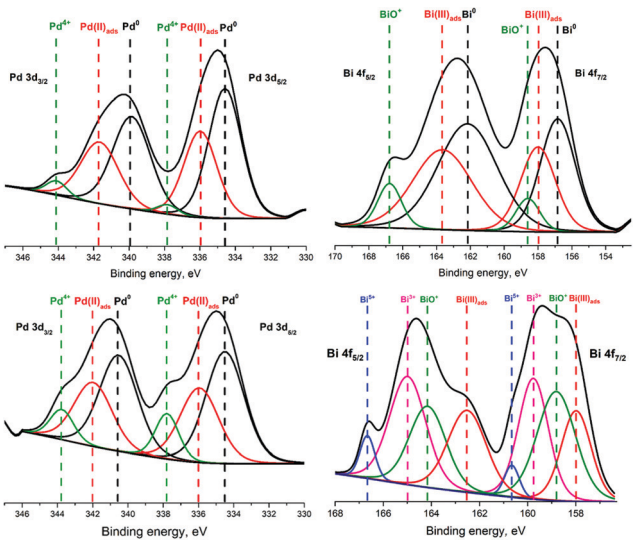

Fig. 12 XPS patterns of the Pd 3d and Bi 4f states for the Pd3 : Bi1 sample after the first (a and b) and fourth (c and d) run.

In a weakly basic medium, in addition to the BiO^+ ion, the component $Bi(H_2O)_3(OH)_3$ may be present. It is also possible that not only monomeric ions and complexes exist, but also polymer particles. The hexameric octahedral complex $[Bi_6(OH)_{12}]^{6+}$ was proposed as a hydrolytic polymer form of the BiO^+ ion, its equilibrium reaction is shown below:[64]

$$n\mathrm{Bi}^{3+} + n\mathrm{H_2O} \leftrightarrows (\mathrm{BiO})_n^{n+} + 2n\mathrm{H}^+$$

In the XPS patterns, the presence of BiO^+ is represented by a peak with a binding energy of 158.6 eV.[63]

The glucose conversion increase observed during the second catalytic cycle can be explained in terms of XPS. The positive effect from the addition of bismuth is achieved only at a certain amount that would create an intensive intermetallic interaction without significant blockage of active centers. The actual Pd : Bi ratio before the first catalytic experiment equals 2.12 while this ratio before the second experiment is 3.06. Presumably, maintaining the 3 : 1 Pd : Bi ratio is responsible for the growth of catalytic activity during the second act. Apart from the above-mentioned electronic interaction between two metals, the ensemble effect may also play a role: the decreasing bismuth content may lead to better conditions for glucose adsorption on active centres.[65]

The XPS profile for the Pd $3d_{5/2}$ state after the 4th catalytic cycle peaks at 334.5, 336.0, and 337.9 eV, corresponding to the Pd^0, $Pd(II)_{ads}$, and Pd^{2+} phases, respectively, which is identical to the phase composition of the catalyst after the first catalytic act. The decrease in the activity of the sample during the fourth act can be associated, first, with a decrease in the palladium content on the surface (from 1.23 at% before the catalytic tests to 0.31 at% after the fourth cycle), which leads to a decrease in the number of active centres, and, secondly, with the increase of the Pd^{2+} phase percentage.

For the Bi $4f_{7/2}$ state, after the 4th catalytic cycle, formation of the Bi^{3+} and Bi^{5+} phases was observed; they correspond to the peaks at 159.8 and 160.7 eV.

As after the first catalytic cycle, the $Bi(III)_{ads}$ and BiO^+ phases are present (158.0 and 158.8 eV, respectively) and the Bi0 phase is absent. Despite the significant losses of bismuth (from 0.58 at% before the catalytic tests to 0.04 at% after the fourth cycle), the activity of the bimetallic sample remains higher than that for monometallic Pd/Al_2O_3 (47.3% of glucose conversion for the bimetallic sample after the fourth cycle *versus* 29.1% for the monometallic sample studied previously[40]). At such a small amount of bismuth, an increase in the activity of palladium due to its protection from oxidation is unlikely. Presumably, it is the electronic interaction between metals that leads to increased activity.

Conclusions

This work highlights the following points:

(I) Particles of Pd/Al_2O_3 and Pd3 : $Bi1/Al_2O_3$ samples with an average size of ~4 nm have shown catalytic activity in the glucose oxidation reaction. According to the XPS patterns, the metal phases Pd^0 and Bi^0 predominate, however, partially oxidized states of metals are observed due to their strong interaction with oxygen atoms of the support. Palladium and bismuth undergo further oxidation during the reaction to Pd^{2+}, BiO^+, Bi^{3+}, and Bi^{5+} states.

(II) The catalyst showed the highest performance at pH 9 and a temperature of 60 °C, since there are no by-products under these conditions. The yield of sodium gluconate was 57% with a selectivity of >99.9%. The reaction temperature increase from 20 °C to 60 °C leads to the higher yield of sodium gluconate without side processes. The catalytic tests at higher temperatures were not conducted because evaporation of the water during the reaction could occur, which could create errors during concentration determination. The calculated activation energy is equal to 67.7 kJ mol^{-1}. At pH ≤ 7, the reaction does not practically proceed. At pH > 10, the formation of a large number of by-products, including fructose,

takes place. A mechanism of catalytic glucose oxidation was proposed, which is a modified mechanism of oxidative dehydrogenation.

(III) A Kinetic study showed that oxygen diffusion to the catalyst's surface does not affect the reaction kinetics at a 500–15 000 [Glu] : [Pd] molar ratio. However, the rate of oxygen dissolution is higher than the rate of the reaction itself. This phenomenon is caused by the additional supply of the oxygen in its molecular form at a high stirring speed.

(IV) The obtained catalysts demonstrated stability and high activity over five catalytic cycles. In the first three catalytic cycles, sodium gluconate was the only product of the oxidation process (yield 57–63%). In the fourth and fifth catalytic cycles, a slight decrease in activity and selectivity ($S \sim$ 94–97%) was observed with a sodium gluconate yield of 44–47%.

Author contributions

M. P. Sandu – conceptualization, data curation, formal analysis, investigation, methodology, visualization, writing – original draft, writing – review & editing; M. A. Kovtunov – conceptualization, data curation, formal analysis, investigation, methodology, visualization, writing – original draft, writing – review & editing; N. V. Gromov – formal analysis, investigation, methodology, writing – original draft; I. A. Kurzina – project administration, resources, supervision, conceptualization, funding acquisition, writing – review & editing, visualization.

Conflicts of interest

There are no conflicts to declare.

Acknowledgements

This research was financially supported by the Competitiveness Improvement Program of the National Research Tomsk State University (Grant no. 8.2.10.2018; sections 'Metal content and texture characterization', 'Investigation by electron microscopy', 'X-ray photoelectron spectroscopy', 'Research of catalytic properties') and the Ministry of Science and Higher Education (Grant no. 0721-2020-0037; section 'Post-catalytic investigation of the Pd3 : Bi1 sample').

Notes and references

1 A. Onda, T. Ochi, K. Kajiyoshi and K. Yanagisawa, *Appl. Catal., A*, 2008, **343**, 49–54.
2 Y. Ikeda, E. Y. Park and N. Okuda, *Bioresour. Technol.*, 2006, **97**, 1030–1035.
3 X. Tan, W. Deng, M. Liu, Q. Zhang and Y. Wang, *Chem. Commun.*, 2009, 7179–7181.
4 M. J. Climent, A. Corma and S. Iborra, *Green Chem.*, 2011, **13**, 520–540.
5 K. Kirimura and I. Yoshioka, in *Comprehensive Biotechnology*, ed. M. Moo-Young, Elsevier, Oxford, 2nd edn, 2011, pp. 143–147.
6 S. Ramachandran, P. Fontanille, A. Pandey and C. Larroche, *Food Technol. Biotechnol.*, 2006, **44**, 185–195.
7 H. Hustede, H. Haberstroh and E. Schinzig, *Ullmann's Encyclopedia of Industrial Chemistry*, Wiley-VCH Verlag, Weinheim, 2000, pp. 37–43.
8 D. T. Sawyer, *Chem. Rev.*, 1964, **64**, 633–643.
9 S. Ramachandran, S. Nair, C. Larroche and A. Pandey, in *Current Developments in Biotechnology and Bioengineering*, ed. A. Pandey, C. Larroche and C. R. Soccol, Elsevier, Oxford, 2017, pp. 577–599.
10 S. Anastassiadis and I. G. Morgunov, *Recent Pat. Biotechnol.*, 2007, **1**, 167–180.
11 A. S. Ahmed, S. S. Farag, I. A. Hassan and H. W. Botros, *J. Radiat. Res. Appl. Sci.*, 2015, **8**, 374–380.
12 T. Roukas, *J. Ind. Microbiol. Biotechnol.*, 2000, **25**, 298–304.
13 N. Vassilev, M. Fenice and F. Federici, *Biotechnol. Tech.*, 1996, **10**, 585–588.
14 S. Barad, S. B. Horovtiz, O. Moskovitz, A. Lichter, A. Sherman and D. Prusky, *Mol. Plant-Microbe Interact.*, 2012, **25**, 779–788.
15 S. Velizarov and V. Beshkov, *Process Biochem.*, 1998, **33**, 527–534.
16 P. Zhou, R. Yao, H. Zhang and J. Bao, *Biotechnol. Bioeng.*, 2019, **116**, 2191–2199.
17 Y. Jiang, K. Liu, H. Zhang, Y. Wang, Q. Yuan, N. Su, J. Bao and X. Fang, *ACS Sustainable Chem. Eng.*, 2017, **5**, 6116–6123.
18 R. Kaur, J. Macleod, W. Foley and M. Nayudu, *Phytochemicals*, 2006, **67**, 595–604.
19 M. Mounir, R. Shafiei, R. Zarmehrkhorshid, A. Hamouda, M. I. Alaoui and P. Thonart, *J. Biosci. Bioeng.*, 2016, **121**, 166–171.
20 B. Nidetzky, M. Fuerlinger, D. Gollhofer, M. Satory, D. Haltrich and K. D. Kulbe, *Ann. N. Y. Acad. Sci.*, 1998, **864**, 446–449.
21 G. S. Erzinger and M. Vitolo, *Appl. Biochem. Biotechnol.*, 2006, **131**, 187–794.
22 S. Anastassiadis, A. Aivasidis and C. Wandrey, *Appl. Microbiol. Biotechnol.*, 2003, **61**, 110–117.
23 S. F. Zhao, H. Jiang, Z. Chi, G. L. Liu, Z. M. Chi, T. J. Chen, G. Yang and Z. Hu, *Antonie van Leeuwenhoek*, 2019, **112**, 669–678.
24 P. Pal, R. Kumar and S. Banerjee, *Chem. Eng. Process.*, 2016, **104**, 160–171.
25 S. Karski, T. Paryjczak and I. Witonñska, *Kinet. Catal.*, 2003, **44**, 618–622.
26 M. Bellardita, E. I. Garcia-López, G. Marcì, B. Megna, F. R. Pomilla and L. Palmisano, *RSC Adv.*, 2015, **5**, 59037–59047.
27 J. Z. Liu, L. P. Weng, Q. L. Zhang, H. Xu and L. N. Ji, *Biochem. Eng. J.*, 2003, **14**, 137–141.
28 P. Vinke, D. de Wit, A. T. J. W. de Goede and H. van Bekkum, *Stud. Surf. Sci. Catal.*, 1992, **72**, 1–20.
29 J. M. H. Dirkx and H. S. van der Baan, *J. Catal.*, 1981, **67**, 1–20.
30 I. Nikov and K. Paev, *Catal. Today*, 1995, **24**, 41–47.
31 X. Liang, C. J. Liu and P. Kuai, *Green Chem.*, 2008, **10**, 1318–1322.
32 Y. Önal, S. Schimpf and P. Claus, *J. Catal.*, 2004, **223**, 122–133.

33 M. Besson, F. Lahmer, P. Gallezot, P. Fuertes and G. Fleche, *J. Catal.*, 1995, **152**, 116–121.
34 S. Karski, T. Paryjczak and I. Witonñska, *Kinet. Catal.*, 2003, **44**, 618–622.
35 I. Witonska, M. Frajtak and S. Karski, *Appl. Catal., A*, 2011, **401**, 73–82.
36 M. Frajtak, I. Witonska, A. Krolak, N. Krawczyk and S. Karski, *Rev. Roum. Chim.*, 2011, **56**, 625–630.
37 A. Abbadi and H. van Bekkum, *J. Mol. Catal. A: Chem.*, 1995, **97**, 111–118.
38 H. Yin, C. Zhou, C. Xu, P. Liu, X. Xu and Y. Ding, *J. Phys. Chem.*, 2008, **112**, 9673–9678.
39 M. P. Sandu, V. S. Sidelnikov, A. A. Geraskin, A. V. Chernyavskii and I. A. Kurzina, *Catalysts*, 2020, **10**, 271.
40 M. P. Sandu, M. A. Kovtunov, V. S. Baturin, I. Kurzina and A. R. Oganov, *Phys. Chem. Chem. Phys.*, 2021, **23**, 14889–14897.
41 H. Wang, Z. Liu, Y. Ma, K. Julian, S. Ji, V. Linkovand and R. Wang, *Phys. Chem. Chem. Phys.*, 2013, **15**, 13999–14005.
42 M. C. Militello and S. J. Simko, *Surf. Sci. Spectra*, 1994, **3**, 387–394.
43 D. L. Mowery, M. S. Graboski, T. R. Ohno and R. L. McCormick, *Appl. Catal., B*, 1999, **21**, 157–169.
44 Y. Huang, Y. Zhang, H. Liu and Z. Gu, Presented in part at the International Symposium on Photoelectronic Detection and Imaging 2011, Bejing, China, August, 2011.
45 B. Zhao, T. Chen, H. Pan, D. Fu and Y. Han, *Physica E*, 2016, **78**, 79–84.
46 M. Womes, T. Cholley, F. Le Petlier, S. Morin, B. Didillon and N. Szydlowski-Schildknecht, *Appl. Catal., A*, 2005, **283**, 9–22.
47 D. Roth, P. Gelin, A. Kaddouri, E. Garbowski, M. Primet and E. Tena, *Catal. Today*, 2006, **112**, 134–138.
48 S. Vajíček, M. Štolcová, A. Kaszonyi, M. Mičušík, P. Alexy, P. Canton, G. Onyestyák, S. Harnos, F. Lónyi and J. Valyon, *J. Ind. Eng. Chem.*, 2016, **39**, 77–86.
49 I. Witońska, A. Królak and S. Karski, *J. Mol. Catal. A: Chem.*, 2010, **331**, 21–28.
50 S. Karski, *J. Mol. Catal. A: Chem.*, 2006, **253**, 147–154.
51 F. A. Al-Odail, A. Anastasopoulos and B. E. Hayden, *Top. Catal.*, 2011, **54**, 77–82.
52 I. G. Casella and M. Contursi, *Electrochim. Acta*, 2006, **52**, 649–657.
53 A. Abbadi, M. Makkee, W. Visscher, J. A. R. van Veen and H. V. Bekkum, *J. Carbohydr. Chem.*, 1993, **12**, 573–587.
54 C. Kooyman, K. Vellenga and H. G. J. De Wilt, *Carbohydr. Res.*, 1977, **54**, 33–44.
55 A. Fan, S. Jaenicke and G. K. Chuah, *Org. Biomol. Chem.*, 2011, **9**, 7720–7726.
56 U. Prüße, M. Herrmann, C. Baatz and N. Decker, *Appl. Catal., A*, 2011, **406**, 89–93.
57 I. V. Delidovich, B. L. Moroz, O. P. Taran, N. V. Gromov, P. A. Pyrjaev, I. P. Prosvirin, V. I. Bujhtiyarov and N. V. Parmon, *Chem. Eng. J.*, 2013, **223**, 921–931.
58 N. V. Gromov, T. B. Medvedeva, K. N. Sorokina, Y. V. Samoylova and Y. A. Rodikova, *ACS Sustainable Chem. Eng.*, 2020, **8**, 18947–18956.
59 M. Wenkin, C. Renard, P. Ruiz, B. Delmon and M. Devillers, *Stud. Surf. Sci. Catal.*, 1997, **108**, 391–398.
60 Y. F. Han, D. Kumar, C. Sivadinarayana, A. Clearfield and D. W. Goodman, *Catal. Lett.*, 2004, **94**, 131–134.
61 T. C. Wen and C. C. Hu, *J. Electrochem. Soc.*, 1993, **140**, 988–995.
62 M. R. Mucalo and C. R. Bullen, *J. Mater. Sci. Lett.*, 2001, **20**, 1853–1856.
63 M. Simões, S. Baranton and C. Coutanceau, *Appl. Catal., B*, 2011, **110**, 40–49.
64 Y. Miao, Z. Yang, X. Liu, L. Xu, L. Ouyang, Y. Gu, H. Chang and R. Ouyang, *Electrochim. Acta*, 2013, **111**, 621–626.
65 T. Mallat and A. Baiker, *Catal. Today*, 1994, **19**, 247–283.

